Simulations of Pulsar Glitches for the Detection of Gravitational Waves

Erik Michael Garcell*
University of Florida - Department of Physics, Gainesville, Florida, U.S.A.

Dr. Hyung Mok Lee, Jinho Kim
Seoul National University - Department of Physics and Astronomy, Seoul, South Korea

(Dated: July 31, 2011)

Simulations of pulsar glitches are conducted in order to determine the probability of detecting gravitational waves produced from these events, using the upcoming gravitational wave detector: Advanced LIGO. Simulations are conducted through pseudo-Newtonian hydrodynamic calculation, allowing for a comprehensive assessment of pulsar excited spherical harmonics and the gravitational wave energies they would produce. Overviews of gravitational waves, the LIGO group, and pulsar glitch mechanisms are given as well as a brief analysis of the formulation of the pseudo-Newtonian hydrodynamics used in simulation. Due to time constraints, the probability of detecting gravitational waves from the pulsar glitch sources could not be conducted. Simulations of the pinned superfluid model of pulsar glithing for high perturbation amplitudes show a linear increase of the exited ${}^2f$ spherical harmonic mode towards lower, and more realistic, perturbations while other modes decay exponentially.

*Electronic address: erikgarcell@phys.ufl.edu

Contents

1. INTRODUCTION

The direct detection of gravitational waves will be a monumental achievement for both physicists and astronomers alike. For physicists, it allows for the direct observation of gravitation in highly relativistic regimes where Einstein's Theory of General Relativity can be tested at it's strong-field limits. For astronomers, gravitational waves will open a door to the outer-cosmos, allowing us to see further into the depths of our universe than has ever been achieved before, and pulsars glitches may be the key to help us do it.

Pulsar glitches are rare and interesting astrological phenomenon, allowing a unique perspective into the structure and dynamics of a neutron star. As well as allowing us to probe the depths of these stars, pulsar glitches also allow us a rare opportunity to detect gravitational waves. Due to their non-radial oscillation, pulsar glitches are capable of emitting periodic gravitational waves that may be within the range of sensitivity of the forthcoming gravitational wave detector, Advanced LIGO.

Though the mechanism behind pulsar glitches is not well understood, there are two competing theories explaining this phenomenon: the star quake model [1] and the pinned superfluid model [2]. In order to determine the likelihood of detecting gravitational waves using Advanced LIGO, hydrodynamic simulations of both these models are conducted.

2. BACKGROUND

2.1. Gravitational Waves

There are two theories pertaining to the natural phenomenon known as gravity. There is Newton's theory of gravity, and Einstein's Theory of General Relativity. According to Newtons theory of gravity, masses feel a gravitational force because all objects in the universe produce a gravitational field. When any mass in the universe changes position its gravitational field, stretching throughout the universe, changes instantaneously as does its associated gravitational force. However, this theory fails to properly explain natural phenomenon occurring around objects with large gravitational fields, such as black holes.

The more commonly accepted description of gravity comes from Einstein's Theory of General Relativity. Already stated in his earlier work on special relativity, Einstein adopted the postulate that the speed of light was the limiting speed of the universe and that no information could be transferred faster than the speed of light. Gravitational fields are a form of information, for they communicate the position of masses in the universe, and so are held to this constraint. Einstein showed in his work that gravitational fields propagate -at the speed of light- and as time-dependent distortions in the fabric of space-time. This propagation of warped space-time is what is called a gravitational wave.

Gravitational waves are generated by time-varying quadrupole moments. In laymen terms, this means that gravitational waves are produced from any accelerating, non-symmetric, object. The reason we have yet to detect these waves is that gravitational waves produced from everyday objects moving with a time-varying quadrupole moment are extraordinarily small. Only relativistic or extremely massive objects produce gravitational waves of any significance, so the only possible source of gravitational waves must come from astrological bodies.

2.2. Advanced LIGO

LIGO (Laser Interferometer Gravitational-Wave Observatory) is a joint project between the California Institute of Technology, the Massachusetts Institute of Technology, funded by the National Science Foundation. The projects ultimate goal is the detection of gravitational waves from astrological sources. The LIGO group currently uses two interferometers to detect these waves, one at Hanford, WA and the other at Livingston, LA [3]. The reasoning behind using more than one detector and location is to verify and locate the source of a detected gravitational wave. If a gravitational wave is detected at one location a detector at the other location should sense the same gravitational wave -travelling at the speed of light- milliseconds later. This helps validate the detection of a gravitational waves by eliminating false positives; if one detector has a reading, but the other does not, the reading can be ignored, but if both detectors do have a reading, due to the time delay between detectors, the relative location of the source of the gravitational wave can be deduced.

Gravitational waves distort space transverse to their propagation [4]. This distortion affects matter by stretching the space between matter along one direction, and contracting it along the orthogonal direction, along the transverse plain of the wave. So to detect gravitational waves an interferometer is used to exactly measure distances between two sets of two points, the later two being orthogonal to the first two, in hopes of seeing the distance between one set stretch and the other contract.

An interferometer is so named because it is a device used to interfere waves. The LIGO interferometer's are L-shaped devices that split a single laser beam in two and send these beams down the two perpendicular arms of the detector. At the ends of each of these arms are two suspended mirrors where the split laser beam can reflect back and forth, gaining intensity, and return back down the arms to intersect with its other half. The wavelengths of the two laser beams, upon intersection, interfere with one another. The phase of the lasers are dependent on the distance travelled by the lasers, and so if the distance travelled by the two laser beams are the same, then the phases of the two beams will be the same. If the phases of any two colliding waves are the same, they will undergo destructive interference and completely cancel out. The two laser beams completely cancel out leaves no light to be observed by the photo-detector situated at the end of the intersecting beams, indicating that no gravitational wave has been detected (Fig:1).

A gravitational wave incident on one of LIGO's detectors would cause the lengths of one of the arms of the device to stretch while causing the other to contract. This would result in a difference in phase between the two interfering laser beams, causing the beams to not completely cancel each other, allowing some light from the beams to hit the photo-detector. This experiment is simple in principle but difficult in practice because the amount of stretching and contraction that would occur for an incident gravitational wave is minute, around the order of 10^{-18} meters for the current detector set-up [5]. Because of this, the interferometer detector must be very sensitive and great pains must be taken to eliminate unwanted vibrations in the system, but that's not the only reason one would want to increase the systems sensitivity.

Gravitational waves propagate through space virtually unaffected by interfering masses or gravitational fields, but they do dissipate as they travel, much like a ripple in a stream. The level of sensitivity of the interferometer is what determines the kinds of gravitational wave sources we are able to detect, and how far these sources can be for the detectors to detect their waves. In order to increase our scope of detection, the level of sensitivity of the

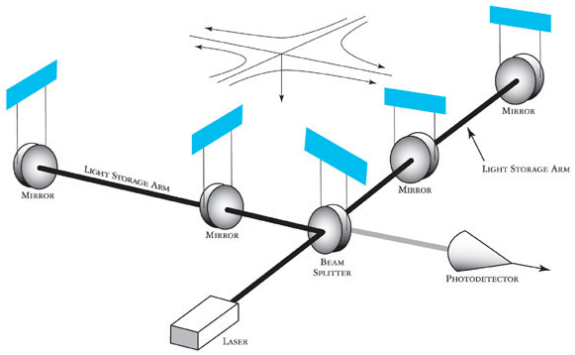

FIG. 1: Diagram of a basic interferometer illustrating one method of noise reduction: the hanging of mirrors by thread in order to isolate them from seismic disturbances. The diagram also depicts an incident gravitational wave and its transverse field causing one arm of the detector to stretch while the other contracts, causing the intersecting laser phases to differ, allowing light to hit the photo-detector.

interferometers must be increased. The current LIGO project's detectors has a range of sensitivity from 40Hz to 200Hz, but up till now no gravitational waves have yet been detected. With new technologies at their disposal, the LIGO group is currently under way on the next generation of gravitational wave detectors, to be called Advanced LIGO. This revamp to the LIGO detectors, slated to start its experimental run in 2015, will raise the sensitivity of the LIGO detectors by a factor of ten in the range of maximum sensitivity: 100Hz-200Hz, while also bringing the lower limit down to 10Hz, thus allowing the detectors to pear out at 1000 times as many galaxies than it had before (Fig:2) [3]. With the completion of Advanced LIGO so close at hand, and with only a handful of theorised sources for gravitational waves, we wish to calculate the likelihood of detecting gravitational waves from one of the more promising sources we know of: pulsar glitches.

2.3. Pulsar Glitches

Pulsars are rapidly rotating neutron stars that emit radiation along their magnetic axis'. The rotation of a neutron stars cause the magnetic fields, contained in these stars, to form electric fields. Electrons, passing through these electric fields, are accelerated and give off radiation. Though radiation from a pulsar is emitted at a constant rate, the reason behind the "pulses" of a pulsar are due to a misalignment of the magnetic axis of the neutron star and its rotational axis (Fig:3). As the star rotates, radiation emitted along the stars magnetic axis periodically cross Earth's line of sight, causing observers on Earth to see a "light house effect". The period of rotation of pulsars gradually decreases over time, but occasionally show a sudden increases, or "glitch".

Though first discovered in 1969, occurring in the Vela pulsar (PSR 0833 -45), pulsar glitches are astrological phenomenon that are not well understood, but are characterised by a sudden increase in rotational frequency followed by a relaxation period where the pulsar returns to its pre-glitch state (Fig:4) [6] . The fractional increase in angular velocity of glitches is typically of the order of $\triangle\Omega\ /\Omega = 10^{-9}$ to 10^{-6}, the time-scale for which ranges

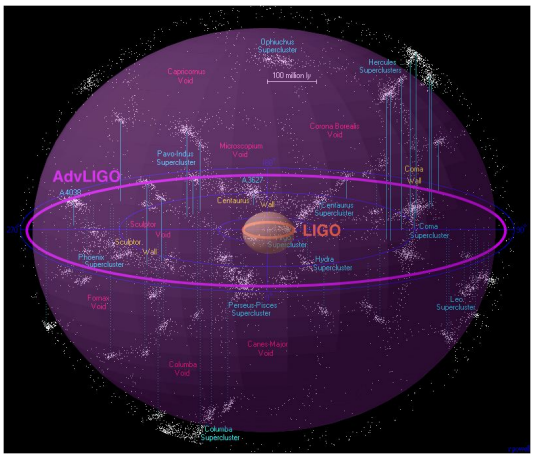

FIG. 2: Scaled model illustrating the reach of Advanced LIGO (purple), as compared to LIGO (orange), where each white dot represents a galaxy and where specific notable regions of local space are marked. Advanced LIGO with its factor of 10 increase in sensitivity is able to see 10 times farther into the cosmos and thus have a volume of detection 1000 times greater than that of LIGO.

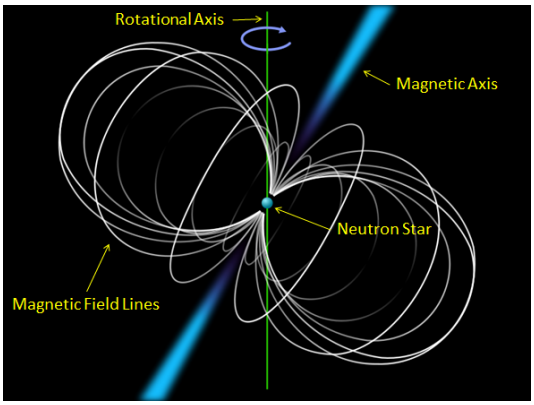

FIG. 3: Illustration of a pulsar depicting the neutron star, it's magnetic field, and its incongruous rotational and magnetic axis.

from a few minutes to a few hours; the relaxation period of a pulsar glitch occurs over a much longer time-scale, ranging from months to years [7].

The rotational energy gained during a pulsar glitch can be as much as $10^{36}J$, but this increase in energy does not correlate to any change in the electromagnetic signature of the pulsar [7]. This indicates that the cause of glitches in pulsars cannot be contributed to external forces such as electromagnetic torques, but must instead be caused by internal forces. The two models explaining the sudden increase in rotational frequency of a pulsar are the starquake model and the pinned superfluid model.

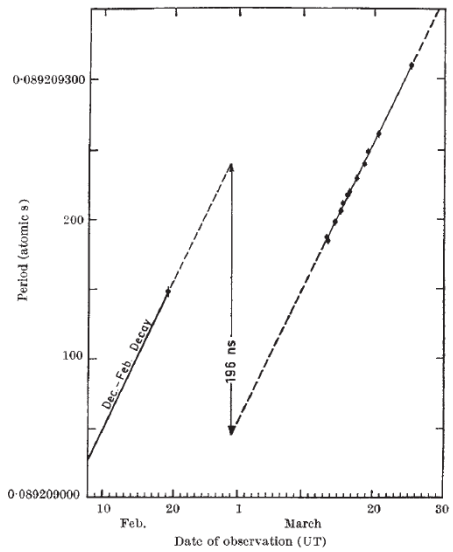

FIG. 4: Data of the first pulsar glitch recorded, taken from the Vela pulsar (PSR 0833 -45). Data clearly shows a sudden acceleration, or decrease in rotational period, and a gradual return to its pre glitch period.

3. MODELS OF PULSAR GLITCHES

Theoretically determined from neutron density and the interior temperature, and observationally confirmed using post-glitch relaxation time-scales, it is evident that neutron stars contain superfluid interiors [7]. For neutron stars this superfluid interior acts as an angular momentum reservoir. As the angular momentum of a pulsar spins down, a differential rotation develops between the crust and superfluid layers since the spin-down rate of the superfluid is slower than the crust. The two different models of pulsar glitches differ from this point on.

The star quake model explains pulsar glitches to be caused by a sudden cracking, or quake, of the neutron stars solid outer shell. The crust of a neutron star is a rigid layer that floats atop a neutron-proton liquid core; as the neutron stars angular momentum spins down, the different rotation between the crust and superfluid layers causes stress on the crust. Eventually the crust will crack and reform, during which the moment of inertia for the star is suddenly decreased. In order to conserve angular momentum, the stars angular velocity must increase, causing a glitch.

The pinned superfluid model explains that the neutron superfluid vortices are pinned to the lattice of the crust. As the differential rotation of crust and superfluid layers increases, the superfluid layer will unpin causing a sudden exchange of inertia from the inner superfluid layer, to the outer crust layer. This exchange of inertia causes the stars angular momentum to spike, or in other words, causes the pulsar to glitch.

4. GLITCH SIMULATIONS

Simulations of pulsar glitches are conducted by pseudo-Newtonian hydrodynamic simulation of normal pulsars using code formulated by Jinho Kim of Seoul National University [9]. The use of hydrodynamic analysis for the simulation of pulsar glitches is unique. Typically, those wishing to simulate pulsar glitches, for use in examining the gravitational waves they may produce, use the perturbation method; the perturbation method approximates the hydrodynamic equations necessary for the analysis of pulsar glitches. The use of the perturbation method allows high resolution solutions to be computed, but in order to use this method one must first assume which of the pulsars spherical harmonic modes is most likely to produce the gravitational waves one wishes to analyse. The reasoning behind our method of simulating the full pseudo-Newtonian hydrodynamic set of equations is to not be constrained by the necessity of assuming which of our pulsars spherical harmonic modes would produce the highest gravitational wave energy. Simulating for the full set of hydrodynamic equations, however, does take more computing power to simulate, and so the resolution of our solutions are not as high as those simulations performed using the perturbation method. Our method, though lower in resolution than the perturbation method, allows for all the spherical harmonic modes of the pulsar to be calculated, allowing us to analyse and compare all the modes as well as select out the mode that will produce the largest gravitational wave.

4.1. Sudo-Newtonian Formulation

The pseudo-Newtonian assumption used in the hydrodynamic simulations calculated assume weak fields by linearising the Einstein equations. Though it would be ideal to solve the complete set of Einstein equations, the computing power, as well as the time needed to do so, make it disadvantageous for us to pursue. Though the full set of equations are not solved for, preliminary simulations demonstrate an agreement between our code and general relativistic results, even for compact neutron stars [9].

The pseudo-Newtonian formulation of our simulations assume the following 3+1 metric,

$$ds^2 = -(1+2\Phi)dt^2 + (1+2\Phi)^{-1}\delta_{ij}dx^i dx^j \tag{1}$$

describing space-time with only one dynamic variable: Φ (gravitational potential). This space-time metric is needed to analyse the energy-momentum tensor of an ideal gas, and its active mass density:

$$T^{\mu\nu} = \rho_0 h u^\mu u^\nu + P g^{\mu\nu} \tag{2}$$

$$\rho_{active} = T - 2T_0^0 = T_i^i - T_0^0 = \rho_0 h \frac{1+v^2}{1-v^2} + 2P \tag{3}$$

where T is the trace of the energy-momentum tensor, ρ_0 is the mass density, P is the pressure, u^μ is the four velocity of a fluid element, $g_{\mu\nu}$ is the assumed 3+1 space-time metric, and h is the specific enthalpy defined as:

$$h = 1 + \epsilon + \frac{P}{\rho_0} \tag{4}$$

From this, the following conservative variables can be defined:

$$\begin{aligned} D &= \rho_0 W \\ S_i &= \rho_0 h W^2 v_i \\ \tau &= \rho_0 h W^2 - P - D \end{aligned} \tag{5}$$

where $W = 1/\sqrt{1-\gamma_{ij}v^i v^j}$ [10]. Using these conservative variables, the hydrodynamic equations for our assumed space-time metric becomes:

$$\frac{\partial(\sqrt{\gamma}q)}{\partial t} + \frac{\partial(\sqrt{-g}f^i)}{\partial x^i} = \sqrt{-g}\Sigma \tag{6}$$

for which the conservative variables q, fluxes f^i, and the source terms Σ are defined as:

$$q = \begin{bmatrix} D \\ S_j \\ \tau \end{bmatrix} \tag{7}$$

$$f^i = \begin{bmatrix} D(v^i - \frac{\beta^i}{\alpha}) \\ S_j(v^i - \frac{\beta^i}{\alpha}) + P\delta^i_j \\ \tau(v^i - \frac{\beta^i}{\alpha}) + Pv^i \end{bmatrix} \tag{8}$$

$$\Sigma = \begin{bmatrix} 0 \\ T^{\mu\nu}(\partial_\mu g_{\mu j} - \Gamma^\lambda_{\mu\nu} g_{\lambda j}) \\ \alpha(T^{\mu 0}\partial_\mu(ln\alpha) - \Gamma^0_{\mu\nu}T^{\mu\nu}) \end{bmatrix} \tag{9}$$

where $\sqrt{-g} = \alpha\sqrt{\gamma}$ [10]. Taking this hydrodynamic equation and using now a cylindrical coordinate system (R, Z, ϕ), our assumed space-time metric becomes:

$$ds^2 = -(1+2\Phi)dt^2 + \frac{1}{1+2\Phi}(dR^2 + dZ^2 + R^2 d\phi^2) \tag{10}$$

for which $\alpha = \sqrt{1+2\Phi}$ and $\beta^i = 0$. Using this new metric, a redefinition of the conservative variables can be completed, allowing our hydrodynamic equation to be recast as:

$$\frac{\partial(\sqrt{\gamma}q)}{\partial t} + \frac{\partial(\sqrt{-g}f^R)}{\partial R} + \frac{\partial(\sqrt{-g}f^Z)}{\partial Z} = \sqrt{-g}\Sigma \tag{11}$$

where $\sqrt{\gamma} = R(1+2\Phi)^{-3/2}$, $\sqrt{g} = R(1+2\Phi)^{-1}$, and where the conservative variables q, fluxes f^R and f^Z, and the source terms Σ are now defined to be:

$$q = \begin{bmatrix} D \\ S_R \\ S_Z \\ S_\Phi \\ \tau \end{bmatrix} \tag{12}$$

$$f^R = \begin{bmatrix} Dv^R \\ S_R v^R + P \\ S_Z v^R \\ S_\Phi v^R \\ \tau v^R + P v^R \end{bmatrix} \tag{13}$$

$$f^Z = \begin{bmatrix} Dv^Z \\ S_R v^Z \\ S_Z v^Z + P \\ S_\Phi v^Z \\ \tau v^Z + P v^Z \end{bmatrix} \tag{14}$$

$$\Sigma = \begin{bmatrix} 0 \\ \frac{-\rho_{active}}{1+2\Phi}\frac{\partial \Phi}{\partial R} + \frac{S_\Phi v^\Phi}{R} + \frac{P}{R} \\ \frac{-\rho_{active}}{1+2\Phi}\frac{\partial \Phi}{\partial Z} \\ 0 \\ S_R \frac{\partial \Phi}{\partial R} + S_Z \frac{\partial \Phi}{\partial Z} \end{bmatrix} \tag{15}$$

[9]. Due to axial symmetry in our cylindrical coordinate system, the hydrodynamics equation Σ can be simplified to:

$$\Sigma = \begin{bmatrix} 0 \\ 0 \\ \frac{-\rho_{active}}{1+2\Phi}\frac{\partial \Phi}{\partial Z} \\ 0 \\ S_R \frac{\partial \Phi}{\partial R} + S_Z \frac{\partial \Phi}{\partial Z} \end{bmatrix} \tag{16}$$

It is these hydrodynamic equations (11, 12, 13, 14, and 16) that are simulated for in our code. To solve for these hydrodynamic equations of our neutron star system, the finite volume method is used. The finite volume method is a common numerical approach to solving hydrodynamic equations that uses computational grids where each grid enforces the conservation laws of the system and represents a volume averaged hydrodynamic quantity. For a further understanding of how the hydrodynamic code is formulated and solved for, please refer to Jinho Kim's paper on the subject [9].

4.2. Simulating Perturbations

To simulate the two models of pulsar glitches within our hydrodynamic equations, we add perturbations to the calculated normal orbit of our star that mimic the effects the two glitch models would have. Before we begin, two assumptions are made: one being that the crust of a neutron star is 10% of its total radius, and that the contributions of crust effects (such as tension), that are not a part of the star quake theory, are negligible and are so ignored [9].

Simulating for the two different types of pulsar glitches requires three different kinds of perturbation, but every orbital perturbation must first obey the total mass and total angular momentum conservation equations, which must remain constant throughout the time evolution of the star:

$$M_0 = \int \rho_0 W dV = 2\pi \int \frac{\rho_0 W}{(1+2\Phi)^{3/2}} R dR dz \tag{17}$$

$$J = \int S_\phi dV = 2\pi \int \frac{\rho_0 W^2 R^2 \Omega}{(1+2\Phi)^3} R dR dZ \tag{18}$$

The first two kinds of perturbation used correspond to the kinds of perturbation created in the star quake model, while the last is for simulating the perturbation from the pinned superfluid model. The perturbations modelling the star quake model are:

$$\frac{\delta\rho_0}{\rho_0} = \begin{cases} \lambda e^{-(\frac{r-c}{\sigma_1})^2} & \text{if } r \leq c \\ (1+\lambda)e^{-(\frac{r-c}{\sigma_2})^2} - 1 & \text{if } r > c \end{cases} \tag{19}$$

where $\delta\rho_o$ stands for the perturbation of the rest mass density, c is the center of the gaussian profile, σ_1 and σ_2 are the width of the gaussian profile, and

$$\begin{aligned} \tfrac{\delta\rho_0}{\rho_0} &= \begin{cases} \lambda_(M)e^{-(\frac{r-c}{\sigma})^2} & \text{if } r \leq c \\ 0 & \text{if } r > c \end{cases} \\ \tfrac{\delta\Omega}{\Omega} &= \begin{cases} \lambda_(J)e^{-(\frac{r-c}{\sigma})^2} & \text{if } r \leq c \\ 0 & \text{if } r > c \end{cases} \end{aligned} \tag{20}$$

for which $c = 1 - \lambda$, and λ is the intensity of perturbation. Both these asymmetric gaussian laws simulate the shifting of the neutron star surface that mimics what occurs in the star quake model when the forces caused by the differential rotational between the superfluid and crust layers cause the crust to crack.

The third type of perturbation used is used to simulate the effects of the pinned superfluid model upon our neutron star simulation. This model simulates rotating velocities near the surface of the neutron star by assuming an angular momentum transfer from the center of the star to the surface without changing the density profile of the star. This mimics the transfer of angular momentum caused by vortex unpinning between internal superfluid boundaries in the pinned superfuid model. This perturbation is expressed as:

$$\begin{aligned} \tfrac{\delta\rho_0}{\rho_0} &= 0 \\ \tfrac{\delta\Omega}{\Omega} &= \begin{cases} -\lambda_(J)e^{-(\frac{r-c}{\sigma})^2} & \text{if } r \leq c \\ \lambda & \text{if } r > c \end{cases} \end{aligned} \tag{21}$$

4.3. Data Analysis

To determine which spherical harmonic mode is most likely to produce gravitational waves, we use the time series quadrupole moment of the neutron star simulation. For our numerical approach the quadrupole moments are:

$$\begin{aligned} I_{xx} &= \int T_0^0(x^2 - \tfrac{1}{3}r^2)dV = \tfrac{2}{3}\pi \int \tfrac{\tau+D}{(1+2\Phi)^{5/2}}(R^2 - 2Z^2)dRdZ \\ I_{zz} &= \int T_0^0(z^2 - \tfrac{1}{3}r^2)dV = \tfrac{4}{3}\pi \int \tfrac{\tau+D}{(1+2\Phi)^{5/2}}(-R^2 + 2Z^2)dRdZ \end{aligned} \tag{22}$$

[9]. To classify the quadrupole moment modes, we compared our data to the works of others and their analysis of pulsar spherical harmonics [11]. To reduce the noise of the data, and more accurately analyse the discrete modes of our system we first perform a Fourier transform of the quadrupole moment of our system. Once completed, to extract the energy of the gravitational wave one must simply take the third time derivative of the quadrupole moment and use the following relation:

λ (perterbation)	${}^2f$-mode	F-mode	${}^2p_1$-mode	H_1-mode	${}^2p_2$-mode	H_2-mode
$1.0 * 10^{-3}$	5.613e-16	2.623e-17	2.853e-17	3.204e-16	4.611e-18	3.218e-16
$3.3 * 10^{-3}$	5.493e-16	8.561e-17	3.565e-16	8.450e-16	3.742e-17	3.123e-16
$6.6 * 10^{-3}$	3.519e-16	3.078e-16	1.960e-15	2.821e-15	1.881e-16	3.586e-16
$1.0 * 10^{-2}$	1.063e-16	5.671e-16	5.636e-15	6.572e-15	5.248e-16	4.736e-16

TABLE I: Table of peak gravitational wave energies of the different excited spherical harmonic modes simulated. Table shows peak values for four different simulated perturbation amplitudes.

$$E = -\frac{1}{5}\langle \dddot{I}_{ij} \dddot{I}_{ij} \rangle \tag{23}$$

which, for the Fourier transformed quadrupole moment, correlates to:

$$E = -\frac{3}{5}(2\pi f)^6 A^2 \tag{24}$$

[12]. Where A is the amplitude of the Fourier series, and f is the frequency. For a more detailed annalysis of how this equation was formulated see Appendix B (8).

5. RESULTS

Here we show the computed gravitational wave energies for four runs of our simulation. Due to time constraints, only iterations of the pinned superfluid like perturbation were simulated for. The constant variables applied in these simulations are listed in Appendix A (8). The parameter changed for these four simulations was the perturbation amplitude (λ) for which the values of $1.0 * 10^{-3}$, $3.3 * 10^{-3}$, $6.6 * 10^{-3}$, and $1.0 * 10^{-2}$ where simulated for. Realistic values for the perturbation amplitude (λ) are between 10^{-4} and 10^{-9}. The reasoning behind our selection of values between 10^{-2} and 10^{-3} is due to restraints on the level of resolution placed by our use of the computationally intensive pseudo-Newtonian hydrodynamics code.

The unit of time used in these computations is $4.92{*}10^{-3} ms$, which arises as a consequence of our using a set units for calculating the simulations where c-the speed of light, G-the gravitational mass constant, and M_{sun}-solar mass are all equal to 1.

The results of the four simulations illustrated in figures 5, 6, 7, and 8 show the different excited spherical harmonic modes of our simulated pulsar glitches and the gravitational wave energies they would produce. Figures 7 and 8, pertaining to the λ= $6.6 * 10^{-3}$, and $1.0 * 10^{-2}$ simulations, both show the same two modes being excited, those being the ${}^2p_1$ and H_1 modes, with the H_1 mode being the dominant mode in both cases. The other two gravitational wave energy plots (5 and 6), however, are quite dissimilar. Figure 5 shows three excited modes, with the ${}^2f$ mode clearly dominating, while figure 6 shows four excited modes with H_1 being the most prevalent. All modes exept for that of the ${}^2f$ mode show an exponential decay in radiated gravitational wave energy as the perterbaion amplitude decreases; the increasing amplitude of the ${}^2f$ mode as the amplitude of perturbation decreases in value may show that the ${}^2f$ mode holds prevalence as perturbation excitations tend towards more realistic values (Table:I and Figure:9).

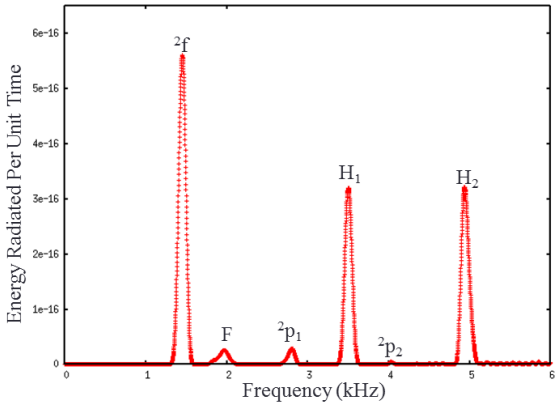

FIG. 5: Gravitational wave energy emitted, per unit time, by the excited spherical harmonic modes produced during a pulsar glitch described by the perturbations of the pinned superfluid model, with perturbation amplitude set to $1.0 * 10^{-3}$. The unit of time for the energy is $4.92 * 10^{-3} ms$.

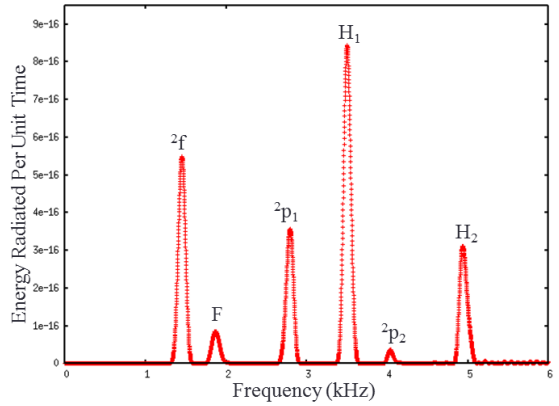

FIG. 6: Gravitational wave energy emitted by the excited spherical harmonic modes produced during a pulsar glitch described by the perturbations of the pinned superfluid model, with perturbation amplitude set to $3.3 * 10^{-3}$. The unit of time for the energy is $4.92 * 10^{-3} ms$.

6. DETECTION

Due to time constraints, the calculation of the damping time of the gravitational wave amplitudes produced from the spherical harmonics of our neutron star simulations could not be completed. The calculation of the damping time is integral in order for one to asses the possibility of detection of a gravitational wave. The longer the damping time, the longer the gravitational wave detectors can integrate the signal over increasing the signal-to-noise ratio and thus increasing the possibility of detection. Without knowing the damping time scale, there is no way to predict whether or not the gravitational wave detector, Advanced LIGO, can detect waves emitted from pulsar glitches.

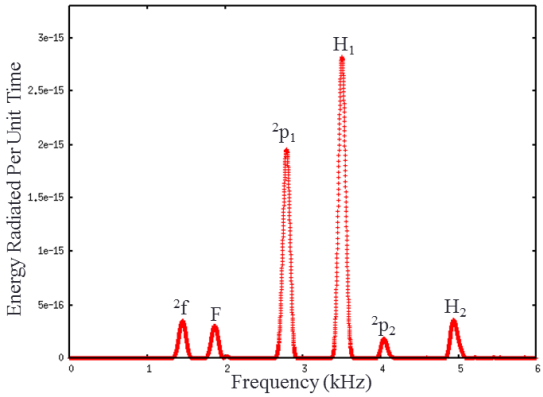

FIG. 7: Gravitational wave energy emitted by the excited spherical harmonic modes produced during a pulsar glitch described by the perturbations of the pinned superfluid model, with perturbation amplitude set to $6.6 * 10^{-3}$. The unit of time for the energy is $4.92 * 10^{-3} ms$.

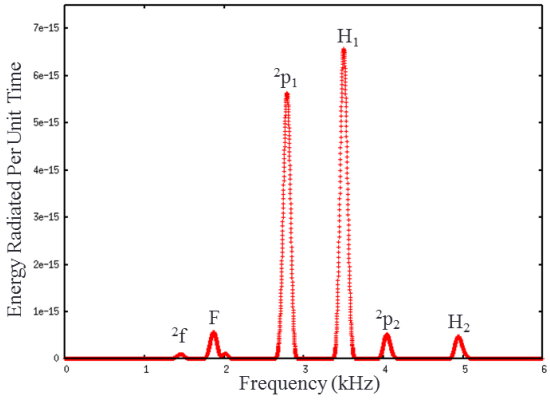

FIG. 8: Gravitational wave energy emitted by the excited spherical harmonic modes produced during a pulsar glitch described by the perturbations of the pinned superfluid model, with perturbation amplitude set to $1.0 * 10^{-2}$.The unit of time for the energy is $4.92 * 10^{-3} ms$.

7. CONCLUSIONS

The ultimate goal of these simulations were to determine the likelihood of detecting gravitational waves from pulsar glitches using the next generation detector, Advanced LIGO. In order to do so, pseudo-Newtonian hydrodynamics code was created to simulate pulsar glitches, determined the excited modes of perturbation, and extract the gravitational wave energy emitted from these mode. The final step, the calculation of the damping time scale for the amplitudes of the gravitational waves could not be completed due to time constraints. Simulations of the pinned superfluid model of pulsar glitching show a near linear dependence in the ^2f-spherical harmonic mode, increasing towards smaller amplitude perturbations, while other modes showed exponential decay. The simulations conducted, being for high

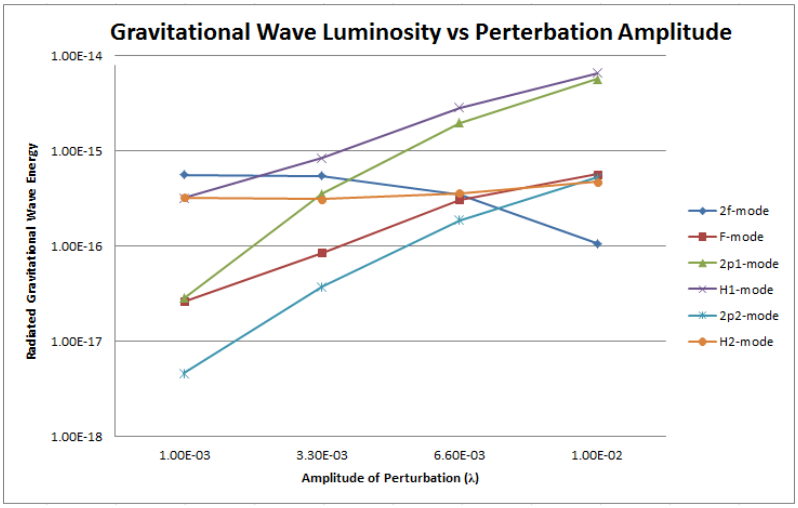

FIG. 9: Log plot showing the exited modes in our simulations of pulsar glitches verses the four perturbation amplitudes simulated for. Simulations mimicked the effect of the pinned supperfluid model of pulsar glitching. The gravitational wave energies are radiated per unit time, the unit of time being $4.92 * 10^{-3} ms$. The figure shows an exponential dependence on the perturbation amplitude for all modes except the ^{f}-mode, which shows an approximate linear correlation.

amplitude perturbations, show that at more realistic values the ^{2}f mode dominates as the predominant source of gravitational waves due to pulsar glitching.

Further simulation, and time, is needed in order to calculate the excited spherical harmonic modes produced from the star quake model of pulsar glitching, as well as calculate the damping time scales of the amplitudes produced from these simulations. Future work hopes to see long damping time scales, allowing the Advanced LIGO detector ample time to integrate the gravitational wave over and subsequently detect these waves.

8. ACKNOWLEDGEMENTS

I would like to thank Dr. Bernard Whiting and Dr. Guido Mueller, of the University of Florida, for selecting me for their IREU (International Research for Undergraduates) program, and allowing me the opportunity to do the work I love while also travelling overseas. I'd like to thank Dr. Hyung Mok Lee, of Seoul National University, for welcoming me to Seoul and accepting me into his lab group, and to Jinho Kim for allowing me the use of his code and for making me feel at home, even when so very far from it. I'd like to also thank Dr. Sang Hoon Oh and Dr. John Oh for welcoming me to Daejeon, and allowing me the use of the NIMS (National Institute for Mathematical Sciences) facilities.

Many thanks also go to Antonis Mytidis, and Kristin Nichola for coordinating this program, and assuring the safe travel of all participants, and last I'd like to thank NSF (The National Science Foundation) for making this program possible, and for funding this research.

[1] M. Ruderman, Nature **223**, 597 (1969), URL http://www.nature.com/nature/journal/v223/n5206/pdf/223597b0.pdf.

[2] N. Anderson, P. W.; Itoh, Nature **256**, 25 (1975), URL http://www.nature.com/nature/journal/v256/n5512/pdf/256025a0.pdf.

[3] G. M. Harry and the LIGO Scientific Collaboration, Classical and Quantum Gravity **27**, 084006 (2010), URL http://stacks.iop.org/0264-9381/27/i=8/a=084006.

[4] R. Barish, B. C.; Weiss, Physics Today **52**, 44 (1999), URL http://www.ligo.caltech.edu/docs/P/P990039-00.pdf.

[5] *Introduction to ligo & gravitational waves*, URL http://www.ligo.org/science/GW-GW2.php.

[6] R. N. Radhakrishnan, V.; Manchester, Nature **222**, 228 (1969), URL http://www.nature.com/nature/journal/v222/n5190/pdf/222228a0.pdf.

[7] G. B. McDonld, Ph.D. thesis, University of Johannesburg (2007), URL http://ujdigispace.uj.ac.za:8080/dspace/bitstream/10210/885/1/Greg%20McDonald%20MSc%20Thesis.pdf.

[8] I. George W. Collins, *The Fundamentals of Stellar Astrophysics* (W.H. Freeman, 2003), URL http://bifrost.cwru.edu/personal/collins/astrobook/AbookC8.pdf.

[9] M. W. C. Jinho Kim, Hee Il Kim and H. M. Lee, department of Physics and Astronomy, FPRD, Seoul National University, Seoul 151-742, Korea. In preperation.

[10] M. Snajdr, department of Physics and Astronomy, University of British Columbia, Vancouver BC, V6T 1Z1 Canada, URL http://142.103.234.164/People/msnajdr/KOREA2006/hydronotes.pdf.

[11] J. A. Font, Monthly Notices of the Royal Astronomical Society **325**, 1463 (2001), URL http://www.astro.auth.gr/~niksterg/papers/FDGS01.pdf.

[12] E. Poisson, Physical Review D **57**, 8 (1997).

Appendices

Appendix A: Parameters Used for Simulation

The variable parameters in our code are listed in the table below, as are the values that where chosen for the four computed simulations. The perturbation amplitude, not listed, is the only independent variable used, all other values for the four iterations of our simulation where kept constant.

Parameters	
Axis Ration	0.750000000000000
Angular Velocity on Axis	1.481338181293601e-2
Angular Velocity at Surface	1.481338181293601e-2
Max $\|\Delta\Omega/\Omega\|$	6.599999999999939e-3
Total Rest Mass (M_0)	1.40000000908893
Total Angular Momentum	1.01617513533747
T	7.526509858163551e-3
Total Proper Mass (M_p)	1.44670798488127
Total Gravitational Mass(M_g)	1.35648708165291
W	9.774741308652812e-2
$T/\|W\|$	7.699958106820609e-2
Time Step (dt)	3.187534208752137e-2

Appendix B: Formulation of Gravitational Wave Energy

Equation 24 calculates gravitational wave energy from the Fourier transform of the quadrupole moment data calculated from pseudo-Newtonian hydrodynamic simulations of pulsar glitches. To understand how one arrives to this equation one must refer back to equation 23, and know the relations:

$$\dddot{I}_{ij}\dddot{I}_{ij} = \dddot{I}^2 = \dddot{I}_{xx}^2 + \dddot{I}_{yy}^2 + \dddot{I}_{zz}^2$$

$$I_{xx} = I_{yy} = -2I_{zz}$$

Using these relations it is easy to see that:

$$\dddot{I}_{ij}\dddot{I}_{ij} = 6\dddot{I}_{xx}^2$$

Plugging this back into equation 23, one gets:

$$E = -\frac{6}{5}\dddot{I}_{xx}^2$$

To get the gravitational wave energy from the Fourier transform of the quadrupole moment, instead of the quadrupole moment itself, one must find a relation between the two. What the Fourier transform does is to isolate the component waves in the quadrupole moment data and separate them into discrete waves of different frequencies. The data output of the Fourier transformed data is the amplitude of the gravitational wave versus the frequency of the wave, so the amplitudes of the Fourier transformed data and the quadrupole moment data are the same. But the energy equation calls for the time derivatives of the quadrupole moment. Taking the time derivative of a wave function is the same as multiplying the wave by $2\pi f$, so for each time derivative of a wave, one must simply multiply the wave by $2\pi f$, where f is the frequency of the wave. One must also remember to take the average of the time derivative, being as that the waves are sinusoidal, and in doing so divide the equation by a factor of two. Applying all of this to the energy equation 23 results in:

$$E = -\frac{6}{5}\frac{[(2\pi f)^3 A]^2}{2}$$

where A is the amplitude of the Fourier transformed data. This can then be easily simplified to the energy equation used for our simulations, equation 24:

$$E = -\frac{3}{5}(2\pi f)^6 A^2$$

Appendix C: Quadrupole Moment Data

Quadrupole moment data (I_{xx}) taken from the four simulation runs completed and documented in this paper.

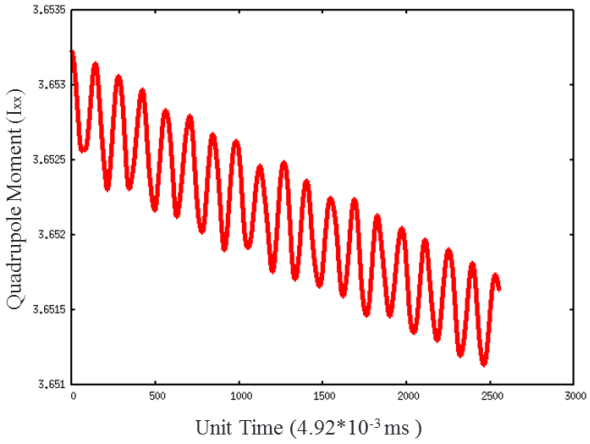

FIG. 10: Quadrupole moment data taken for a pulsar glitch produced by the perturbations modelled by the pinned superfluid theory of pulsar glitches. The quadrupole moment (I_{xx}) was calculated for a pulsar with perturbation amplitude $1.0 * 10^{-3}$.

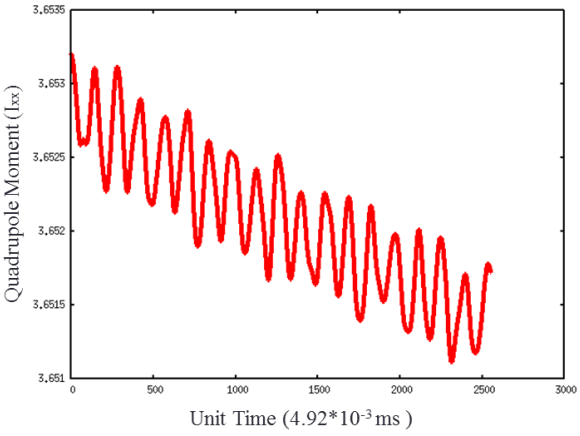

FIG. 11: Quadrupole moment data taken for a pulsar glitch produced by the perturbations modelled by the pinned superfluid theory of pulsar glitches. The quadrupole moment (I_{xx}) was calculated for a pulsar with perturbation amplitude $3.3 * 10^{-3}$.

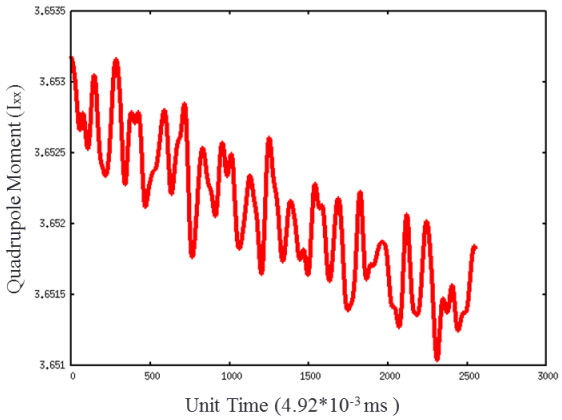

FIG. 12: Quadrupole moment data taken for a pulsar glitch produced by the perturbations modelled by the pinned superfluid theory of pulsar glitches. The quadrupole moment (I_{xx}) was calculated for a pulsar with perturbation amplitude $6.6 * 10^{-3}$.

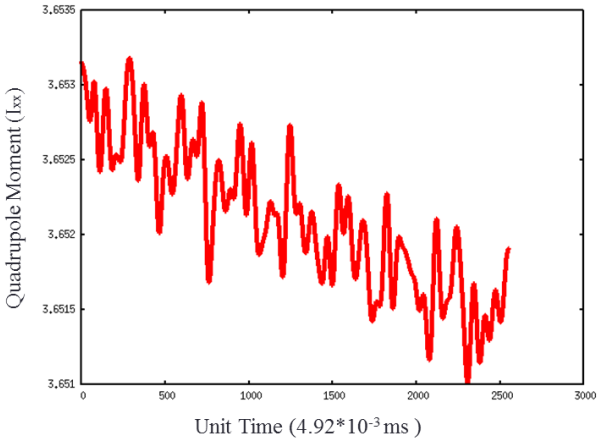

FIG. 13: Quadrupole moment data taken for a pulsar glitch produced by the perturbations modelled by the pinned superfluid theory of pulsar glitches. The quadrupole moment (I_{xx}) was calculated for a pulsar with perturbation amplitude $1.0 * 10^{-2}$.

Appendix D: Fourier Transformed Data

Fourier transform data of the quadrupole moments (I_{xx}) taken from the four simulation runs completed and documented in this paper.

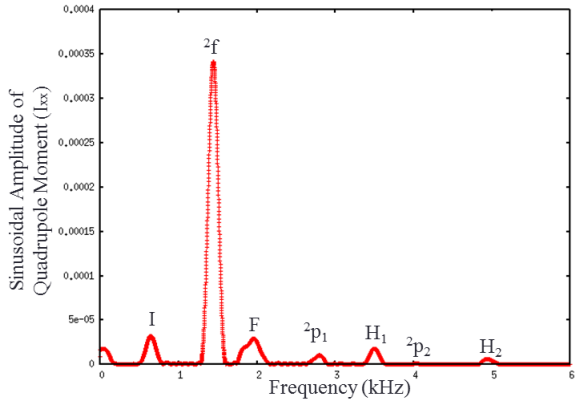

FIG. 14: Fourier transform of the quadrupole moment (I_{xx}) of a pseudo-Newtonian hydrodynamic simulation of a the pinned superfluid theory of pulsar glitches, for which the perturbation amplitude was set to $1.0 * 10^{-3}$.

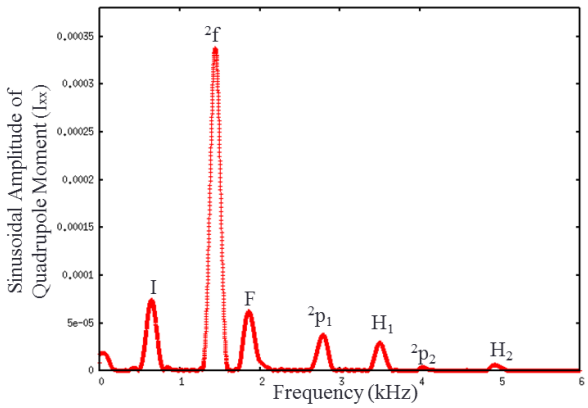

FIG. 15: Fourier transform of the quadrupole moment (I_{xx}) of a pseudo-Newtonian hydrodynamic simulation of a the pinned superfluid theory of pulsar glitches, for which the perturbation amplitude was set to $3.3 * 10^{-3}$.

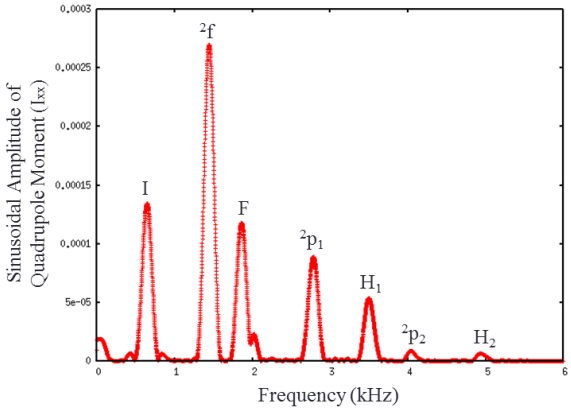

FIG. 16: Fourier transform of the quadrupole moment (I_{xx}) of a pseudo-Newtonian hydrodynamic simulation of a the pinned superfluid theory of pulsar glitches, for which the perturbation amplitude was set to $6.6 * 10^{-3}$.

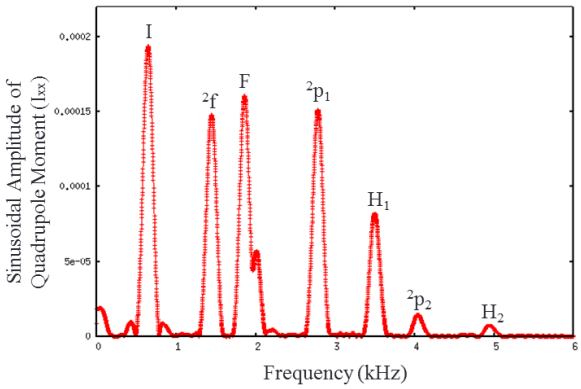

FIG. 17: Fourier transform of the quadrupole moment (I_{xx}) of a pseudo-Newtonian hydrodynamic simulation of a the pinned superfluid theory of pulsar glitches, for which the perturbation amplitude was set to $1.0 * 10^{-32}$.